Available online at www.sciencedirect.com
ScienceDirect
International Journal of Solids and Structures 43 (2006) 7776–7792
INTERNATIONAL JOURNAL OF SOLIDS and STRUCTURES
www.elsevier.com/locate/ijsolstr

Deformation and reverse snapping of a circular shallow shell under uniform edge tension

Jen-San Chen *, Tzu-Min Huang

Department of Mechanical Engineering, National Taiwan University, Taipei, Taiwan 10617, Taiwan

Received 31 August 2005; received in revised form 30 March 2006
Available online 7 April 2006

Abstract

In this paper we study the deformation and stability of a shallow shell under uniform edge tension, both theoretically and experimentally. Von Karman's plate model is adopted to formulate the equations of motion. For a shell with axisymmetrical initial shape, the equilibrium positions can be classified into axisymmetrical and unsymmetrical solutions. While there may exist both stable and unstable axisymmetrical solutions, all the unsymmetrical solutions are unstable. Since the unsymmetrical solutions will not affect the stability of the axisymmetrical solutions, it is concluded that for quasi-static analysis, there is no need to include unsymmetrical assumed modes in the calculation. If the shell is initially in the unstrained configuration, it will only be flattened smoothly when the edge tension is applied. No snap-through buckling is possible in this case. On the other hand, if the shell is initially in the strained position, it will be snapped back to the stable position on the other side of the base plane when the edge tension reaches a critical value. Experiment is conducted on several free brass shells of different initial heights to verify the theoretical predictions. Generally speaking, for the range of initial height $H < 10$ the experimental measurements of the deformation and the reverse snapping load agree well with theoretical predictions.

Keywords: Reverse snapping; Shallow shell; Edge tension

1. Introduction

Snap-through buckling of a shallow shell under transverse loading is a classical mechanics problem, initiated by von Karman and Tsien (1939). Since then this buckling problem has attracted a great deal of research and became recognized as one of the most difficult problems because of the discrepancy between experiment and theory. Many possible factors affecting the accuracy of the theoretical prediction were examined carefully. Huang (1964) has shown that unsymmetrical snapping is possible when the rise parameter of the axisymmetrical shallow shell is moderately high. This consideration of unsymmetrical modes helps partially close the gap

* Corresponding author. Tel.: +886 2 3366 2693; fax: +886 2 2363 1755.
E-mail address: jschen@ntu.edu.tw (J.-S. Chen).

0020-7683/$ - see front matter
doi:10.1016/j.ijsolstr.2006.03.029

between theoretical prediction and experimental measurement. Yamada et al. (1983) investigated the effect of geometrical imperfection and concluded that geometrical imperfection can affect the critical load of the shallow shell considerably. In the case when the pressure load is applied suddenly instead of quasi-statically, the snap-through phenomenon becomes even more complicated. Budiansky and Roth (1962) treated the case of a clamped shell of parabolic revolution under a uniform pressure applied suddenly for a finite time. More references on the static and dynamic critical loads of shallow shells under lateral loading can be found in Simitses' book (1990).

Besides the transverse loading cases discussed above, it was suggested that a shallow shell can also undergo snap-through buckling when it is subjected to in-plane edge tension. Akkas and Odeh (2001) used a linearized finite element incremental-iterative method to study the possibility of snapping a shallow spherical shell with uniform in-plane tension on the outer rim. Only the axisymmetrical deformation is assumed in Akkas and Odeh (2001). Their numerical simulation suggested that for certain narrow range of initial height, snap-through due to uniform edge tension may be possible. For a shell with rise parameter $\lambda = 7.0827$, Akkas and Odeh (2001) presented a graph showing the relation between the edge tension and the calculated apex deflection. The shell apex is above the base plane containing the outer rim before the edge tension is applied. They demonstrated that even before the so-called snap-through occurs, the shell apex has already moved to slightly lower than the base plane. The snap-through action simply brings the apex even lower. This phenomenon is highly peculiar and the validity of their conclusion appears to remain in question.

In another study on the possibility of snap-through buckling of shallow shells under in-plane loading, Chen and Lin (2005) investigated the deformation of a spinning annular non-flat disk. The in-plane loading in this case is the centrifugal force. Both the initial and deformed shapes of the disk are assumed to be axisymmetrical. They concluded that snapping can occur only in one direction, i.e., from the strained state back to the initial state on the opposite side of the base plane when certain critical rotation speed is reached. This one-way snapping from the strained position back to the initial position on the other side may be called "reverse snapping". On the other hand, if the non-flat disk is initially in the unstrained state, it will simply be flattened out due to rotation and no snapping is observed, both in numerical simulation and in experiment. Moreover, the flattened-out disk remains on the same side of the base plane throughout. The main features of the results reported in Chen and Lin (2005) apparently contradict the predictions presented in Akkas and Odeh (2001). It remains unknown whether the differences in these main features are due to the different loading mechanisms in the two problems, or simply because one of the conclusions is incorrect.

The above review gives us motivation to investigate the tension buckling problem of shallow shells in more detail. The goal of this paper is to answer the question whether snap-through from the initial unstrained position to the strained position on the other side of the base plane is possible when the shallow shell is under in-plane edge tension. There are several extensions in this paper compared to the study in Akkas and Odeh (2001). First of all, we employ the von Karman's plate model and use a Galerkin's method to study the deformation of the shallow shell. All the possible solutions, both stable and unstable, are obtained at the same time. Secondly, we include the unsymmetrical assumed-modes in the solution. It is well known that unsymmetrical assumed modes will affect the snapping load prediction when the shallow shell is under lateral force, see Huang (1964). Whether this is also the case in the tension buckling problem is still unknown. Thirdly, experimental work is conducted to compare with the theoretical predictions.

2. Equations of motion

Fig. 1 shows a shallow shell with base radius a under the action of a uniformly distributed in-plane stress resultant p^*. The initial (unstrained) shape of the shell is w_0^*. We assume that the effect of gravity on the shell deformation can be neglected. The equations of motion of the shallow shell in terms of transverse displacement w^* and stress function ϕ^* can be written as

$$\rho h w^*_{,t^*t^*} + D\nabla^{*4}(w^* - w_0^*) = w^*_{,r^*r^*}\left(r^{*-1}\phi^*_{,r^*} + r^{*-2}\phi^*_{,\theta\theta}\right) + \left(r^{*-1}w^*_{,r^*} + r^{*-2}w^*_{,\theta\theta}\right)\phi^*_{,r^*r^*} - 2\left(r^{*-1}w^*_{,\theta}\right)_{,r^*}\left(r^{*-1}\phi^*_{,\theta}\right)_{,r^*} \tag{1}$$

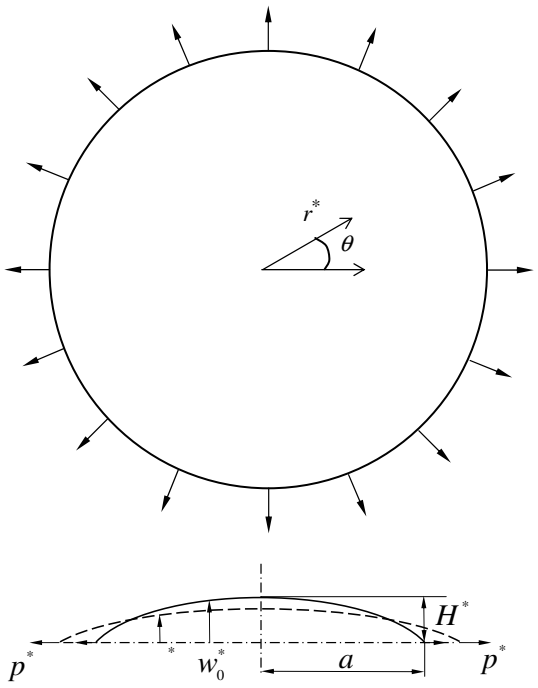

Fig. 1. A shallow shell under uniform edge tension.

$$\nabla^{*4}\phi^* = Eh\left[-w^*_{,r^*r^*}\left(r^{*-1}w^*_{,r^*} + r^{*-2}w^*_{,\theta\theta}\right) + \left(r^{*-1}w^*_{r^*\theta} - r^{*-2}w^*_{,\theta}\right)^2 + w^*_{0,r^*r^*}\left(r^{*-1}w^*_{0,r^*} + r^{*-2}w^*_{0,\theta\theta}\right) - \left(r^{*-1}w^*_{0,r^*\theta} - r^{*-2}w^*_{0,\theta}\right)^2\right] \tag{2}$$

w^* and w^*_0 are measured from the same base plane. (r^*, θ) are polar coordinates. t^* is time. The parameters ρ, h, E, ν, and D are the mass density, thickness, Young's modulus, Poisson ratio, and flexural rigidity of the shallow shell, respectively. In writing Eqs. (1) and (2) the effects of in-plane inertia and shear deformation across the thickness are neglected. The stress function ϕ^* is related to the in-plane stress resultants by

$$N^*_r = r^{*-1}\phi^*_{,r^*} + r^{*-2}\phi^*_{,\theta\theta} \tag{3}$$

$$N^*_\theta = \phi^*_{,r^*r^*} \tag{4}$$

$$N^*_{r\theta} = -\left(r^{*-1}\phi^*_{,\theta}\right)_{,r^*} \tag{5}$$

On the outer edge the in-plane radial stress resultant is equal to p^*, while the in-plane shear stress resultant is zero. Mathematically, the boundary conditions for ϕ^* at $r^* = a$ are

$$r^{*-1}\phi^*_{,r^*} + r^{*-2}\phi^*_{,\theta\theta} = p^* \tag{6}$$

$$\left(r^{*-1}\phi^*_{,\theta}\right)_{,r^*} = 0 \tag{7}$$

In the out-of-plane direction, two types of boundary conditions are considered for the lateral displacement w^*. First we consider the case when the outer rim is free in the lateral direction. Mathematically, the boundary conditions for w^* at $r^* = a$ are

$$(w^* - w^*_0)_{,r^*r^*} + \nu r^{*-1}\left((w^* - w^*_0)_{,r^*} + r^{*-1}(w^* - w^*_0)_{,\theta\theta}\right) = 0 \tag{8}$$

$$-D\left[\left(\nabla^{*2}(w^* - w^*_0)\right)_{,r^*} + (1-\nu)r^{*-2}\left((w^* - w^*_0)_{,r^*} - r^{*-1}(w^* - w^*_0)\right)_{,\theta\theta}\right] + p^* w^*_{,r^*} = 0 \tag{9}$$

In writing Eq. (9) we assume that the direction of the edge tension remains unchanged when the shell deforms. In other words, the edge tension is conservative. The reason we study the case of free outer rim is that it is easier to accomplish in the experiment as described later.

Secondly, we consider the case of simply-supported outer rim. In this case Eq. (9) will be replaced by

$$w^* - w_0^* = 0 \tag{10}$$

The reason we study the case of simply-supported boundary condition is to compare our result with that presented in Akkas and Odeh (2001). In all these cases, both w^* and ϕ^* are required to be finite at the center $r^* = 0$.

Eqs. (1) and (2) can be non-dimensionalized by introducing the following dimensionless quantities (without superposed asterisk):

$$t = \frac{t^*}{a^2}\sqrt{\frac{D}{\rho h}}, \quad r = \frac{r^*}{a}, \quad (w^*, w_0^*) = \frac{1}{h}(w^*, w_0^*), \quad \phi = \frac{\phi^*}{D}$$

$$(p, N_r, N_\theta, N_{r\theta}) = \frac{a^2}{D}\left(p^*, N_r^*, N_\theta^*, N_{r\theta}^*\right)$$

After substituting these relations into Eqs. (1) and (2) we can rewrite the equations of motion in the following dimensionless forms:

$$\begin{aligned} w_{,tt} + \nabla^4(w - w_0) = {} & w_{,rr}\left(r^{-1}\phi_{,r} + r^{-2}\phi_{,\theta\theta}\right) + \phi_{,rr}\left(r^{-1}w_{,r} + r^{-2}w_{,\theta\theta}\right) \\ & - 2\left(r^{-1}w_{,\theta}\right)_{,r}\left(r^{-1}\phi_{,\theta}\right)_{,r} \end{aligned} \tag{11}$$

$$\begin{aligned} \nabla^4\phi = {} & 12(1-\nu^2)\Big[-w_{,rr}(r^{-1}w_{,r} + r^{-2}w_{,\theta\theta}) + \left(r^{-1}w_{,r\theta} - r^{-2}w_{,\theta}\right)^2 \\ & + w_{0,rr}\left(r^{-1}w_{0,r} + r^{-2}w_{0,\theta\theta}\right) - \left(r^{-1}w_{0,r\theta} - r^{-2}w_{0,\theta}\right)^2\Big] \end{aligned} \tag{12}$$

where

$$\nabla^2 \equiv \frac{\partial^2}{\partial r^2} + \frac{1}{r}\frac{\partial}{\partial r} + \frac{1}{r^2}\frac{\partial^2}{\partial\theta^2}, \quad \nabla^4 \equiv \nabla^2\nabla^2$$

For the case when the outer edge is free in the out-of-plane direction the in-plane loading p appears in the boundary condition (9). We can rewrite the equations of motion and boundary conditions so that the in-plane loading appears in the governing equation and is absent in the boundary conditions. We first define the displacement field u as

$$u = w - w_0 \tag{13}$$

In doing so, the governing equations can be rewritten into the form,

$$\begin{aligned} u_{,tt} + \nabla^4 u = {} & (u + w_0)_{,rr}(r^{-1}\phi_{,r} + r^{-2}\phi_{,\theta\theta}) + \left[r^{-1}(u + w_0)_{,r} + r^{-2}(u + w_0)_{,\theta\theta}\right]\phi_{,rr} \\ & - 2\left[r^{-1}(u + w_0)_{,\theta}\right]_{,r}(r^{-1}\phi_{,\theta})_{,r} - p\delta(r-1)(u + w_0)_{,r} \end{aligned} \tag{14}$$

$$\begin{aligned} \nabla^4\phi = {} & 12(1-\nu^2)\Big[-u_{,rr}(r^{-1}u_{,r} + r^{-2}u_{,\theta\theta}) + (r^{-1}u_{,r\theta} - r^{-2}u_{,\theta})^2 \\ & + 2(r^{-1}u_{r\theta} - r^{-2}u_{,\theta})(r^{-1}w_{0,r\theta} - r^{-2}w_{0,\theta}) - w_{0,rr}(r^{-1}u_{,r} + r^{-2}u_{,\theta\theta}) - u_{,rr}(r^{-1}w_{0,r} + r^{-2}w_{0,\theta\theta})\Big] \end{aligned} \tag{15}$$

$\delta(\bullet)$ is the Dirac delta function. The free boundary conditions for u and ϕ at $r = 1$ are

$$u_{,rr} + \nu r^{-1}(u_{,r} + r^{-1}u_{,\theta\theta}) = 0 \tag{16}$$

$$(\nabla^2 u)_{,r} + (1-\nu)r^{-2}(u_{,r} - r^{-1}u)_{,\theta\theta} = 0 \tag{17}$$

$$r^{-1}\phi_{,r} + r^{-2}\phi_{,\theta\theta} = p \tag{18}$$

$$(r^{-1}\phi_{,\theta})_{,r} = 0 \tag{19}$$

It is noted that the edge tension p has been moved from the boundary condition to the equation of motion (14).

For the case of simply-supported shell, the last term containing $p\delta(r-1)$ in Eq. (14) is dropped, while the boundary condition (17) is replaced by

$$u = 0 \tag{20}$$

It is noted that while Eqs. (14) and (15) are nonlinear in terms of w, they are linear in ϕ. Therefore we can divide the stress function ϕ in Eq. (15) into two parts,

$$\phi = \phi_1 + \phi_2 \tag{21}$$

The first part ϕ_1 accounts for the edge load effect. It satisfies the homogeneous equation

$$\nabla^4 \phi_1 = 0 \tag{22}$$

and the inhomogeneous boundary condition (18). ϕ_1 can be solved readily as

$$\phi_1 = \frac{pr^2}{2} \tag{23}$$

On the other hand, the second part ϕ_2 satisfies the same inhomogeneous equation as Eq. (15) but subject to the boundary condition (18) with $p = 0$. After substituting Eqs. (21) and (23) back to Eqs. (14) and (15) we can rewrite the equations of motion in the following form for the case of a free shell:

$$\begin{aligned} &u_{,tt} + \nabla^4 u - r^{-1}[pr(u+w_0)_{,r}]_{,r} - r^{-2}p(u+w_0)_{,\theta\theta} \\ &\quad = (u+w_0)_{,rr}(r^{-1}\phi_{2,r} + r^{-2}\phi_{2,\theta\theta}) + [r^{-1}(u+w_0)_{,r} + r^{-2}(u+w_0)_{,\theta\theta}]\phi_{2,rr} \\ &\qquad - 2[r^{-1}(u+w_0)_{,\theta}]_{,r}(r^{-1}\phi_{2,\theta})_{,r} - p\delta(r-1)(u+w_0)_{,r} \end{aligned} \tag{24}$$

$$\begin{aligned} \nabla^4 \phi_2 = 12(1-\nu^2)\Big[&-u_{,rr}(r^{-1}u_{,r} + r^{-2}u_{,\theta\theta}) + (r^{-1}u_{,r\theta} - r^{-2}u_{,\theta})^2 \\ &+ 2(r^{-1}u_{r\theta} - r^{-2}u_{,\theta})(r^{-1}w_{0,r\theta} - r^{-2}w_{0,\theta}) - w_{0,rr}(r^{-1}u_{,r} + r^{-2}u_{,\theta\theta}) - u_{,rr}(r^{-1}w_{0,r} + r^{-2}w_{0,\theta\theta})\Big] \end{aligned} \tag{25}$$

Again, for the case of simply-supported shell, the last term containing $p\delta(r-1)$ in Eq. (24) is dropped.

In the following we assume that the initial shape w_0 is axisymmetrical and has a maximum height H at the center. Therefore, we can write

$$w_0(r) = H\bar{w}_0(r) \tag{26}$$

where the relative height between apex and outer rim of $\bar{w}_0(r)$ is chosen to be 1, i.e., $\bar{w}_0(0) - \bar{w}_0(1) = 1$. In the next section we describe the Galerkin's method used to discretize the equations of motion (24) and (25) only for the case of a free shell. For the other case of a simply-supported shell, the procedure is similar.

3. Galerkin's method

In order to solve the coupled nonlinear Eqs. (24) and (25), we expand u and ϕ_2 in terms of assumed modes u_{mn} and ϕ_{mn} as following:

$$u(r,\theta,t) = \sum_{m=0}^{\infty}\sum_{n=0}^{\infty} c_{mn}(t)u_{mn}(r,\theta) \tag{27}$$

$$\phi_2(r,\theta,t) = \sum_{m=0}^{\infty}\sum_{n=0}^{\infty} d_{mn}(t)\phi_{mn}(r,\theta) \tag{28}$$

u_{mn} and ϕ_{mn} satisfy the equations

$$\nabla^4 u_{mn} - \alpha_{mn}^4 u_{mn} = 0 \tag{29}$$

$$\nabla^4 \phi_{mn} - \beta_{mn}^4 \phi_{mn} = 0 \tag{30}$$

and the same homogeneous boundary conditions as u and ϕ_2 do. Subscripts m and n represent the number of nodal circles and nodal diameters, respectively. u_{mn} and ϕ_{mn} can be expressed in the following forms:

$$u_{mn}(r,\theta) = R_{mn}(r)\cos n\theta$$
$$\psi_{mn}(r,\theta) = S_{mn}(r)\cos n\theta$$

u_{mn} can be interpreted as the bending vibration modes of a flat disk. The general solution of R_{mn} and S_{mn} can be written in the forms,

$$R_{mn} = A_1 J_n(\alpha_{mn} r) + A_2 I_n(\alpha_{mn} r)$$
$$S_{mn} = B_1 J_n(\beta_{mn} r) + B_2 I_n(\beta_{mn} r)$$

J_n and I_n are Bessel functions of the order n. A_i and B_i are constants determined from the boundary conditions. Fig. 2 shows the first few assumed modes of R_{mn} and S_{mn}. Their corresponding eigenvalues can be found in Tables 1a and 1b.

In solving the eigenvalues special care has to be taken for the cases with $n = 0$ and 1. For the axisymmetrical mode with $n = 0$, the boundary condition Eq. (19) will be satisfied automatically. To fix the problem that we

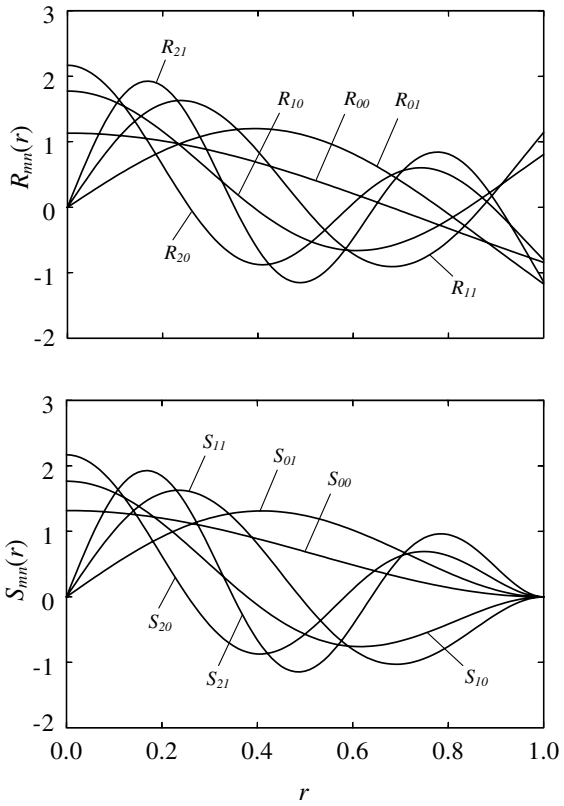

Fig. 2. Radial functions R_{mn} and S_{mn} of the assumed modes used in Galerkin's method.

Table 1a
Eigenvalues α_{mn}

α_{mn}	$n = 0$	$n = 1$	$n = 2$
$m = 0$	3.00052	4.52488	2.31481
$m = 1$	6.20026	7.73380	5.93802
$m = 2$	9.36751	10.90676	9.18511

Table 1b
Eigenvalues β_{mn}

β_{mn}	$n=0$	$n=1$	$n=2$
$m=0$	3.19622	4.61090	5.90568
$m=1$	6.30644	7.79927	9.19688
$m=2$	9.43950	10.95807	12.40222

have only one physical boundary condition for ϕ in this case, we use a trivial condition $\phi=0$ at $r=1$. It is noted that the stress resultants will not be changed by adding any arbitrary constant to the stress function. For the case with $n=1$, Eqs. (18) and (19) will result in the same equation, so we also use the trivial condition $\phi=0$ at $r=1$ to replace Eq. (19). It can be proved mathematically and verified numerically that both u_{mn} and ϕ_{mn} are orthonormal in the sense that

$$\int_0^{2\pi}\int_0^1 u_{ij}u_{mn}r\,\mathrm{d}r\,\mathrm{d}\theta=\delta_{im}\delta_{jn} \tag{31}$$

$$\int_0^{2\pi}\int_0^1 \phi_{ij}\phi_{mn}r\,\mathrm{d}r\,\mathrm{d}\theta=\delta_{im}\delta_{jn} \tag{32}$$

δ_{mn} is the Kronecker delta symbol.

After substituting Eqs. (27) and (28) into Eq. (25), multiplying both sides by ϕ_{pq} and integrating, we obtain

$$d_{pq}=\sum_{k=0}^{\infty}\sum_{s=0}^{\infty}\left(c_{ks}H\Psi_{pqks}+\sum_{l=0}^{\infty}\sum_{j=0}^{\infty}c_{ks}c_{lj}\Psi_{pqkslj}\right) \tag{33}$$

where

$$\Psi_{pqkslj}=\frac{-12(1-\nu^2)}{\beta_{pq}^4}\int_{\theta=0}^{2\pi}\int_{r=0}^{1}S_{pq}\Big[R_{ks,rr}(r^{-1}R_{lj,r}-r^{-2}j^2R_{lj})\cos(s\theta)\cos(j\theta)\cos(q\theta)$$
$$+(-r^{-2}sjR_{ks,r}R_{lj,r}+r^{-3}sj(R_{ks}R_{lj})_{,r}-r^{-4}sjR_{ks}R_{lj})\sin(s\theta)\sin(j\theta)\cos(q\theta)\Big]r\,\mathrm{d}r\,\mathrm{d}\theta$$

$$\Psi_{pqks}=\frac{-12(1-\nu^2)\pi\delta_{sq}}{\beta_{pq}^4}\int_{r=0}^{1}S_{pq}[r^{-1}(R_{ks,r}\bar{w}_{0,r})_{,r}-r^{-2}s^2R_{ks}\bar{w}_{0,rr}]r\,\mathrm{d}r$$

After substituting Eqs. (33), (27) and (28) into Eq. (24), multiplying by u_{mn} and integrating, we then obtain

$$\ddot{c}_{mn}+K_{mn}=0 \tag{34}$$

where

$$K_{mn}=\alpha_{mn}^4c_{mn}+pH\Lambda_{mn}+p\sum_{f=0}^{\infty}\sum_{g=0}^{\infty}c_{fg}\Lambda^{(1)}_{mnfg}-H\sum_{p=0}^{\infty}\sum_{q=0}^{\infty}\sum_{k=0}^{\infty}\sum_{s=0}^{\infty}\left(c_{ks}H\Psi_{pqks}+\sum_{l=0}^{\infty}\sum_{j=0}^{\infty}c_{ks}c_{lj}\Psi_{pqkslj}\right)\Lambda^{(2)}_{mnpq}$$
$$-\sum_{f=0}^{\infty}\sum_{g=0}^{\infty}\sum_{p=0}^{\infty}\sum_{q=0}^{\infty}\sum_{k=0}^{\infty}\sum_{s=0}^{\infty}\left(c_{ks}H\Psi_{pqks}+\sum_{l=0}^{\infty}\sum_{j=0}^{\infty}c_{ks}c_{lj}\Psi_{pqkslj}\right)c_{fg}\Lambda_{mnksfg} \tag{35}$$

The constants Λ_{mn}, $\Lambda^{(1)}_{mnfg}$, $\Lambda^{(2)}_{mnpq}$, and Λ_{mnfgpq} are defined as

$$\Lambda_{mn}=2\pi\delta_{n0}\int_0^1 R_{mn,r}\bar{w}_{0,r}r\,\mathrm{d}r$$

$$\Lambda^{(1)}_{mnfg}=\pi\delta_{gn}\int_0^1\left[R_{mn,r}R_{fg,r}+R_{mn}g^2r^{-2}R_{fg}\right]r\,\mathrm{d}r$$

$$\Lambda^{(2)}_{mnpq}=\pi\delta_{qn}\int_0^1 R_{mn}[r^{-1}(\bar{w}_{0,r}S_{pq,r})_{,r}-\bar{w}_{0,rr}r^{-2}q^2S_{pq}]r\,\mathrm{d}r$$

$$\Lambda_{mnfgpq} = \int_0^{2\pi}\int_0^1 R_{mn}\Big\{\Big[r^{-1}(R_{fg,r}S_{pq,r})_{,r} - r^{-2}(q^2R_{fg,rr}S_{pq} + g^2R_{fg}S_{pq,rr})\Big]\cos(g\theta)\cos(q\theta)\cos(n\theta) - 2gq(r^{-1}R_{fg})_{,r}(r^{-1}S_{pq})_{,r}\sin(g\theta)\sin(q\theta)\cos(n\theta)\Big\}r\,\mathrm{d}r\,\mathrm{d}\theta$$

In the case of static analysis the acceleration terms in Eq. (34) can be neglected. The expression of K_{mn} in Eq. (35) is formidable as it contains eight looped summations in general. However, close inspection of the system of equations reveals that the equations can be divided into two groups; one involves only unsymmetrical assumed modes and the other involves both axisymmetrical and unsymmetrical assumed modes. If there are M axisymmetrical assumed modes and N unsymmetrical assumed modes used in the expansions (27) and (28), then Eq. (34) represents $M+N$ coupled nonlinear equations. For the N equations corresponding to the unsymmetrical modes (i.e., those equations in (34) with subscript $n \neq 0$), the constant term in Eq. (34) is zero. Therefore, these are N homogeneous equations. On the other hand, the remaining M equations can be rearranged into the form

$$F(c_{m0}) + G(c_{mn}) = 0 \tag{36}$$

Every term in the group $F(c_{m0})$ contains only the coordinate c_{m0}, and can be expressed as the following:

$$F(c_{m0}) = \alpha_{m0}^4 c_{m0} + pH\Lambda_{m0} + p\sum_{f=0}^{\infty} c_{f0}\Lambda^{(1)}_{m0f0} - H\sum_{p=0}^{\infty}\sum_{k=0}^{\infty}\left(c_{k0}H\Psi_{p0k0} + \sum_{l=0}^{\infty} c_{k0}c_{l0}\Psi_{p0k0l0}\right)\Lambda^{(2)}_{m0p0} - \sum_{f}^{\infty}\sum_{p=0}^{\infty}\sum_{k=0}^{\infty}\left(c_{k0}H\Psi_{p0k0} + \sum_{l=0}^{\infty} c_{k0}c_{l0}\Psi_{p0k0l0}\right)c_{f0}\Lambda_{m0k0f0} \tag{37}$$

The group $G(c_{mn})$ in Eq. (36) contains coordinates c_{mn}, in which n can be zero or non-zero. More importantly, each term in group $G(c_{mn})$ contains at least one c_{mn} with $n \neq 0$. Since the N equations corresponding to the unsymmetrical modes are homogeneous, they admit one type of solution with all $c_{mn(n\neq 0)} = 0$. For such type of solution Eq. (36) can be reduced to

$$F(c_{m0}) = 0 \tag{38}$$

This implies that the axisymmetrical solutions will not be affected by the addition of unsymmetrical assumed modes in expansions (27) and (28). This property is due to the fact that the initial shape is assumed to be axisymmetrical. On the other hand, if the initial shape is no longer axisymmetrical, then there will not be purely axisymmetrical deformations. Similar property can also be observed in the problem of a pinned sinusoidal arch under prescribed end motion, in which the steady state deformations can be classified into one-mode solutions (symmetrical) and two-mode solutions (unsymmetrical), see Chen and Liao (2005).

It is noted that the shallow shell under conservative edge tension constitutes a conservative system. Therefore, the energy method based on Ritz approximation should be applicable. The formulation based on the energy method has been worked out in detail in Huang (2006). The resulted equilibrium equations indeed agree with the discretized equation (34) derived above.

4. Equilibrium positions of a clamped shell under uniform pressure

Before presenting the results of the behavior of a shallow shell under edge tension, we shall first re-do the classical problem of a clamped shell under uniform pressure. The critical load of this problem has been solved by Huang (1964) with a different method. The two governing equations for this problem are similar to Eqs. (24) and (25), except that Eq. (24) is modified to

$$u_{,tt} + \nabla^4 u + q = (u+w_0)_{,rr}(r^{-1}\phi_{2,r} + r^{-2}\phi_{2,\theta\theta}) + [r^{-1}(u+w_0)_{,r} + r^{-2}(u+w_0)_{,\theta\theta}]\phi_{2,rr} - 2[r^{-1}(u+w_0)_{,\theta}]_{,r}(r^{-1}\phi_{2,\theta})_{,r} \tag{39}$$

The relation between the dimensionless pressure q and the physical pressure q^* is

$$q = \frac{a^4 q^*}{Dh} \tag{40}$$

The method presented in the previous section can be readily modified to solve this problem. The initial shape of the shell is assumed to be spherical as in Huang (1964),

$$\bar{w}_0 = 1 - r^2 \tag{41}$$

Fig. 3 shows the apex position $w(0)$ as a function of q for a shell with initial height $H = 5.51$. The Poisson ratio is assumed to be 1/3. Twelve assumed modes are used in the calculation, they are u_{mn} with $m = 0$–3 and $n = 0$–2. As the pressure q increases from zero, the apex position lowers gradually. We use solid and dashed lines to represent stable and unstable solutions. The stability of these positions is determined by the usual perturbation technique, for example, see Chen and Lin (2005). If only the axisymmetrical assumed modes (u_{m0}) are used in the expansion, the apex position will trace the locus ABCD, and snap-through will occur at point B ($q = 1571$). In other words, the locus AB is stable while the locus BCD is unstable. If one-nodal-diameter modes are appended in the expansion, then additional unsymmetrical positions corresponding to locus EF will appear. The intersection of loci EF and AB at point E will change the stability of the axisymmetrical solutions such that locus EB will become unstable. Therefore, snapping will occur at point E. If the two-nodal-diameter modes are appended in the expansion, the additional locus FHIG will appear. This additional locus intersects the locus AB at points I and G. The intersection I does not change the stability of the locus AB while the intersection G changes the locus GE from stable to unstable. Therefore, snapping will occur at an even smaller load at point G. Adding the modes with more than two nodal diameters will not change the critical load because the additional intersection points are all on the right hand side of point G. Fig. 3 shows clearly that unsymmetrical assumed modes can indeed affect the critical load prediction in a clamped shell under uniform pressure. It will be of interest to see whether this is also the case for a shell under uniform edge tension, as will be discussed in the next section.

Although Huang (1964) did not present the load–deformation diagram like Fig. 3, he did predict the critical loads numerically. The non-dimensionalization scheme in Huang (1964) is different from the one adopted in the current paper. In Huang (1964) the initial height parameter λ and pressure q_H are defined as

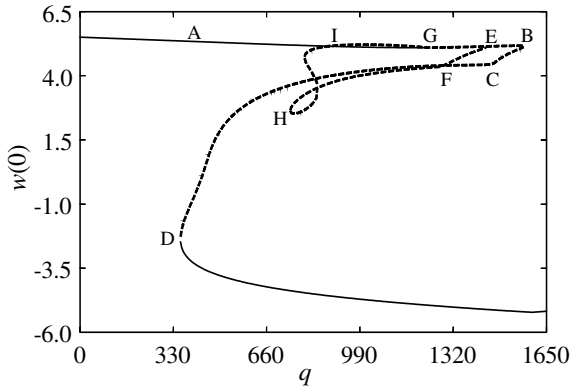

Fig. 3. Apex position $w(0)$ of a clamped shell under uniform pressure q.

Table 2
Effect of the addition of unsymmetrical assumed modes ($n = 1$ and 2) on the critical load q of a clamped shell under uniform pressure, predicted in Huang (1964) and the current paper, respectively

q	$n = 0$	$n = 1$	$n = 2$
Huang (1964)	1579	1459	1230
Current paper	1571	1441	1229

The column with $n = 0$ represents the critical load prediction by using only axisymmetrical assumed modes.

$$\lambda = 2[3(1-\nu^2)]^{1/4}\left(\frac{H^*}{h}\right)^{1/2}, \quad q_H = \frac{\lambda^2 a^4 q^*}{32EH^{*3}h} \tag{42}$$

Therefore, the initial height $H = 5.51$ in Fig. 3 corresponds to $\lambda = 6$ in Huang (1964). By translating the critical loads in Huang (1964) into the dimensionless q used in this paper we can compare Huang's predictions with ours in terms of q in Table 2. It appears that our numerical results agree quite well with the predictions in Huang (1964).

5. Equilibrium positions of a free shell under edge tension

In this section we investigate the deformation and stability of a shallow shell under uniform edge tension. The outer rim is assumed to be free of support in the lateral direction. The reason for choosing this support condition is that it is easier to realize in the experiment. With the hope that the first few modes in the expansions (27) and (28) will dominate the solutions, we assume that the initial shape of the shell is in the form of the fundamental mode shape $u_{00}(r)$,

$$\bar{w}_0 = \frac{u_{00}(r)}{u_{00}(0) - u_{00}(1)} \tag{43}$$

The maximum physical radial slope of the initial shape is $Hh/a\bar{w}_{0,r}(1)$ at the outer rim. In order for the plate Eqs. (1) and (2) to be acceptable, the maximum slope has to be small. Fig. 4(a) shows the relation between the apex position relative to the outer rim position and the edge tension for a shell with initial height $H = 4.5$. The Poisson ratio is chosen to be 0.3. In the case when the shell deforms axisymmetrically, the outer rim remains a circle. Therefore, the ordinate of Fig. 4(a) can be interpreted as the apex position relative to the base plane containing the outer rim. On the other hand, if the shell deforms unsymmetrically, the outer rim becomes a spatial curve. In such a case the outer rim position is referred to the position at $\theta = 0$. In Fig. 4(a) we use five assumed modes in the expansions (27) and (28), they are $(0,0)$, $(1,0)$, $(0,1)$, $(1,1)$, and $(0,2)$. The first number in the mode label represents the number of nodal circles, and the second number represents the number of nodal diameters. Therefore, the modes $(0,0)$, $(1,0)$ are axisymmetrical assumed modes, while the rest are unsymmetrical. The results from the five-mode approximation in Fig. 4(a) for $H = 4.5$ are compared with a 9-mode approximation adding modes $(2,0)$, $(2,1)$, $(1,2)$, $(0,3)$ in the solution expansion. We found that adding 4 more assumed modes in the expansion only produces negligible difference compared with the original five-mode approximation. With this convergence test we can be sure that all the possible equilibrium positions have been obtained.

Fig. 4(a) shows that when the shell is free of edge tension, i.e., $p = 0$, there exist five equilibrium positions. Among these five positions, three are axisymmetrical, denoted by the labels P_s^1, P_s^1, and P_s^3, respectively. The subscript "s" signifies that the equilibrium positions contain only the axisymmetrical assumed modes. The superscripts denote the sequence number of these axisymmetrical solutions from top to bottom. The other two equilibrium positions are unsymmetrical solutions, denoted by P_u^1, P_u^2. Among these five positions only two are stable, i.e., P_s^1 and P_s^3. All the unsymmetrical solutions are unstable. As the edge tension increases, the stable P_s^3 merges with the unstable P_s^2 via a saddle-node bifurcation at $p = 7.2$. On the other hand, the two unsymmetrical solutions merge at $p = 5.6$. To show the contribution of the five assumed modes in Fig. 4(a) on the final solution, we also present the relation between coordinates c_{mn} and the edge tension p in Fig. 4(b)–(f).

Fig. 5 shows the equilibrium positions for a shell with larger initial height $H = 6$ via a 7-mode approximation. The assumed modes used in the expansion are $(0,0)$, $(1,0)$, $(2,0)$, $(0,1)$, $(1,1)$, $(2,1)$, and $(0,2)$. In the case when $p = 0$, there are a total of 9 equilibrium positions, among them five are axisymmetrical and four are unsymmetrical. Most of the solutions are unstable, except the two axisymmetrical solutions P_s^1 and P_s^5. The deformation behavior in Fig. 5 is similar to Fig. 4, only more complicated.

Our experience in convergence test shows that the need for more modes in ensuring convergence is mostly to settle the unsymmetrical solutions. For the axisymmetrical solutions, which are independent of the unsymmetrical assumed modes, the number of modes needed to ensure convergence is much smaller. Moreover, the stable axisymmetrical solutions converge even faster than the unstable axisymmetrical solutions.

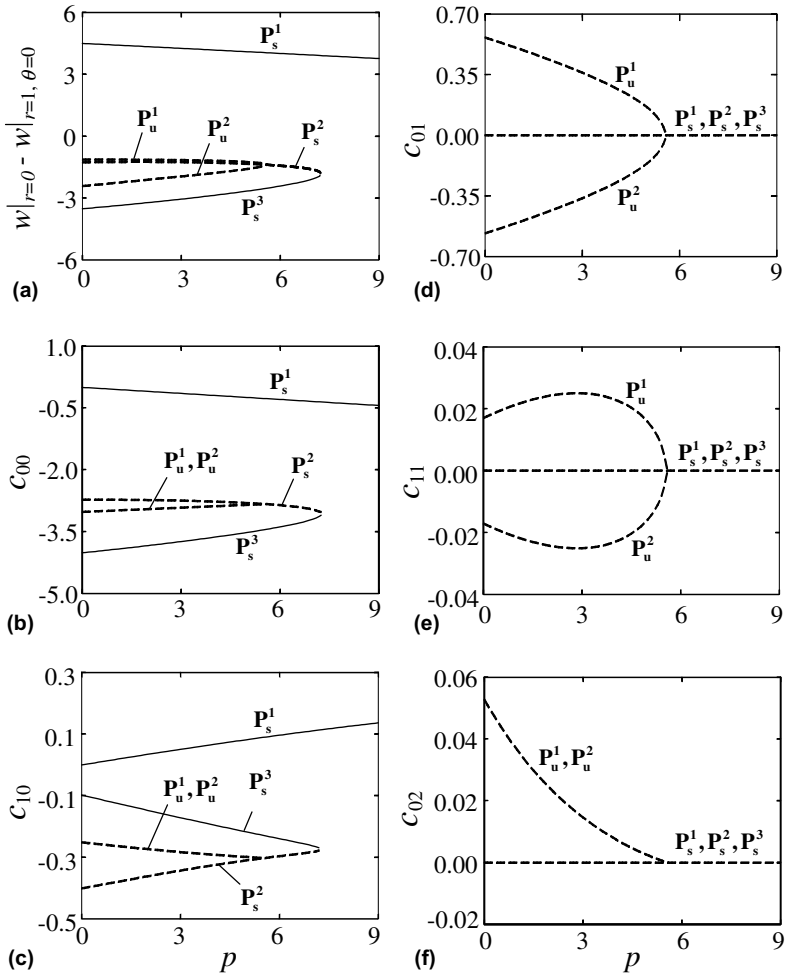

Fig. 4. (a) Apex position relative to the outer-rim plane for a free shell with $H = 4.5$ under uniform edge tension p. (b)–(f) Coordinates c_{mn} as functions of p.

After observing Figs. 4 and 5 carefully several comments can be made. (1) From Fig. 4(d)–(f), we clearly see that for the symmetrical solutions P_s^1, P_s^2, and P_s^3 the coordinates c_{01}, c_{11}, and c_{02} corresponding to the unsymmetrical assumed modes are indeed zero. Furthermore, the two unsymmetrical solutions P_u^1 and P_u^2 contain both axisymmetrical and unsymmetrical assumed modes. These results confirm our previous analysis in Section 3. (2) For the two unsymmetrical solutions P_u^1 and P_u^2 all the coordinates c_{mn} are identical except that the coordinates c_{01} and c_{11} are opposite in sign. Therefore, these two positions are in fact the mirror images of each other. In other words, these two unsymmetrical positions are actually the same. (3) The interception of the unsymmetrical solution loci (P_u^1 and P_u^2) and the symmetrical solution locus (P_s^2) at $p = 5.6$ does not change the stability property of either locus. In other words, the inclusion of the unsymmetrical assumed modes in the expansion does not change the position and stability of the symmetrical solutions. This is in contrast to the situation when the shell is under lateral force, in which the loci interception may change the stability of the solutions as demonstrated in the last section. (4) The loci of the unsymmetrical solutions cease to exist after meeting the locus of the axisymmetrical solution because the coordinates c_{01} and c_{11} become complex after the intersection. The above observations lead us to the conclusion that for quasi-static analysis such as the one in this paper, there is no need to include unsymmetrical assumed modes in the solution. This might not be the case for dynamic case though.

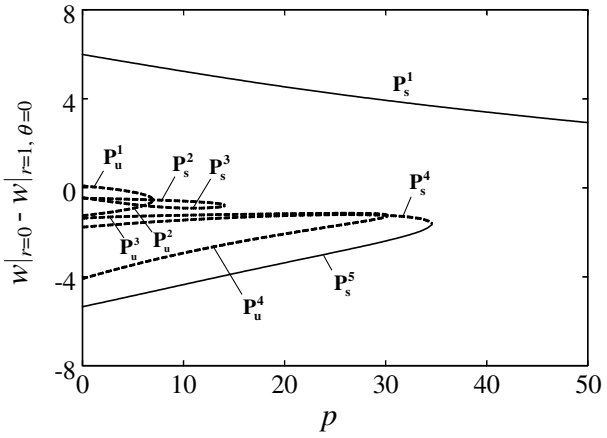

Fig. 5. Apex position relative to the outer-rim plane for a free shell with $H = 6$ under uniform edge tension p.

6. Reverse snapping edge load

For the case of a free shell, our numerical simulation shows that if the initial height of the free shell is in the range $3.7 < H < 20$, there exist exactly two stable positions. This unique property may be used to design a new bi-stable switch actuated with edge tension. In such an application it will be necessary to know the relation between the reverse snapping load p_{cr} and the initial height H.

By observing Fig. 4(b) and (c) we know that reverse snapping occurs when Eq. (34) admits a double root, which requires the following derivative determinate to vanish:

$$\det\left|\frac{\partial K_{mn}}{\partial c_{pq}}\right| = 0 \tag{44}$$

Therefore, if there are N assumed modes used in the expansion, the order of the determinant in Eq. (44) will be N by N. By using Eqs. (34) and (44) we can then solve for p_{cr} and the corresponding coordinates c_{mn}. Fig. 6 shows the relation between p_{cr} and the initial height H. Only axisymmetrical assumed modes are used in the calculation. N represents the number of axisymmetrical modes used in the calculation. It appears that 5 modes are enough to achieve convergence in this calculation because the curve corresponding to $N = 6$ is indistinguishable from the one with $N = 5$. It is noted that for $H = 20$, it requires more than 10 assumed modes to achieve full convergence for every solution. However, the stable solutions converge faster, and as a consequence 5 modes are sufficient to predict the reverse snapping load accurately.

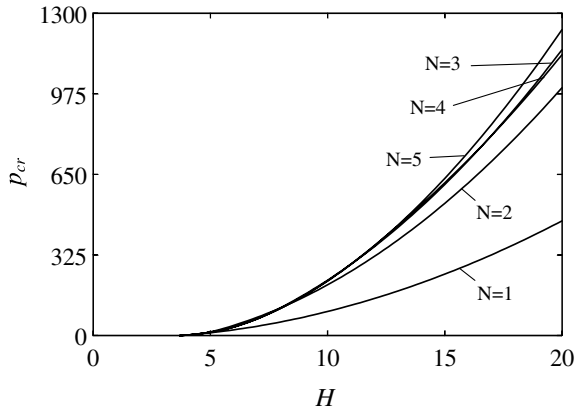

Fig. 6. Relation between the reverse snapping load p_{cr} and the initial height H.

7. Apex position of a simply-supported shell under edge tension

Fig. 4 shows clearly that if the shell is initially in the unstrained position (P_s^1), the edge tension will only flatten the shell smoothly. No snap-through will occur. Moreover, the shell is always on the same side of the base plane no matter how large the edge tension is. In other words, the locus of P_s^1 is always on the positive side. These are in contrast with the conclusions reported in Akkas and Odeh (2001) in which the authors claimed that snap-through is possible and the apex is moved to the other side of the base plane even before the so-called snap-through occurs. Although the shell discussed in Akkas and Odeh (2001) is simply supported and the initial shape is spherical, the main features should be the same. In Fig. 7, we examine the deformation of a simply-supported shell with the same parameters adopted in Akkas and Odeh (2001). Only the branch of solution corresponding to the initial unstrained shape is shown in Fig. 7. The initial height H is 7.68, which corresponds to $\lambda = 7.0827$ in Akkas and Odeh (2001). The Poisson ratio is chosen to be 1/3. The initial shape is in the form of Eq. (41). Four axisymmetrical assumed modes are used in the expansion. For the ease of comparison with Fig. 7 in Akkas and Odeh (2001) we choose the ordinate to be p^*/Eh and the abscissa to be the apex deflection $[w_0^*(0) - w^*(0)]/H^*$. Attention is focused on the region when the apex deflection approaches 1. Apparently, the shell apex remains on the same side of the base plane throughout and the peculiar phenomena reported in Akkas and Odeh (2001) do not appear in our calculation. Furthermore, the edge tension p^*/Eh corresponding to the abrupt upward veering in Fig. 7 is about 0.007, which is only one hundredth of the edge tension reported in Akkas and Odeh (2001). Although we will prove with experiment that our prediction is closer to the truth later, it is interesting to point out that for the edge tension $p^*/Eh = 0.7$ as predicted in Akkas and Odeh (2001), the resulted in-plane stress on the outer rim will exceed 10 times of the yield stress of any metallic sheet.

8. Initial shape measurement

In order to verify the theoretical predictions, we conduct an experiment on the deflection measurement of a shallow shell with axisymmetrical initial shape. The shell is made from a rolled brass sheet with thickness 0.4 mm. The Young's modulus and mass density of the material are 103 GPa and 8864 kg/m^3, respectively, see Ashby and Jones (1980). The outer radius of the shell is designed to be 15 cm. On a circle (with radius 14.7 cm) near the outer rim we drill 18 evenly-spaced small holes (with diameter 3 mm). The initial shape of the disk is designed to approximate the first axisymmetrical mode u_{00}. We first machined a mold of the desired initial shape with two circular steel slabs on the lathe. The flat brass sheet is bent and locked in the mold. The mold together with the bent brass sheet is then put in an oven to heat to 250 °C for 1 h to relieve the internal stresses. In each hole near the outer rim we tie a cotton string. The concave shell is then mounted on a vertical steel slab with 18 short horizontal stubs. Each stub is mounted with a small pulley. The 18 strings

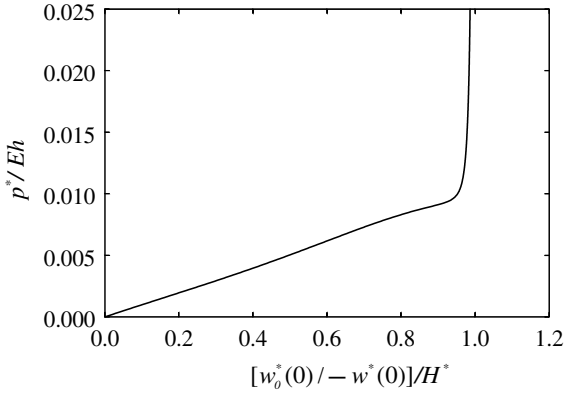

Fig. 7. Relation between the edge tension and apex deflection for a simply supported shell with $H = 7.68$. The apex is on the same side of the outer-rim plane throughout.

are then passed around the pulleys. Plastic bags containing heavy weights are hung at the other ends of the strings to provide tension to the shell. The positions of the stubs on the vertical steel slab are designed in such manner that these tensions will be pointing in the radial direction of the shell. The pulleys on the stubs are to minimize the friction effect. Fig. 8 is a photograph of our experimental setup, which we use to approximate the loading condition of a free shallow shell under uniform tension. The reason we hang the shell in the vertical direction is to avoid the gravitational effect on the shell deformation.

The first step of the experiment is to examine the initial shape of the shallow shell. To obtain a global picture of the actual initial shape of the shallow shell we measure the heights at five radial positions relative to the base plane containing the outer rim. Since the shell is free of support laterally, we have to eliminate the rigid body tilting in our measurement. In order to achieve this we install three micro-stages on a vertical post, which is ensured to be parallel to the vertical steel board. On each micro-stage we attach a metallic probe connected to a multimeter. An alarm will sound off whenever the probe touches the brass shell. The center stage is targeted at the apex of the shell while the other two are targeted at two points on the same diameter and symmetric with respect to the apex. The relative heights between the apex and the two other points can be measured accurately. By averaging these two relative heights, we can then eliminate the rigid body tilting of the free shell. We define this average height as the height at the specific radius. At each radius we make the measurement at 6 diameters evenly divided in the circumferential direction. After measuring the initial shape, the shell is bent by hands gently from the initial unstrained position to the strained position on the other side. The shape of the strained position is measured by the same method. The solid lines in Fig. 9 are the measured mean height and the mean deviation at these five radial positions of the shell. Also shown for comparison are the designed initial shape u_{00} and the theoretical prediction of its strained configuration P_s^3, as represented by dashed lines. The mean height of this shell at the apex is 2.19 mm ($H = 5.47$). The maximum radial slope of the initial shape is calculated to be 0.015, which is small enough to warrant the use of von Karman's plate model. The wavy deviation of this specimen shown in Fig. 9 is about 15% of the axisymmetrical mean height. Although the wavy deviation is not as small as desired, the mean height indeed approximates the theoretical shapes, both in the initial and the strained positions. For convenient reference, we present the measured results with both dimensionless parameters (left and bottom sides) and the physical ones (right and top sides). The same labeling style is adopted in Fig. 10 as well.

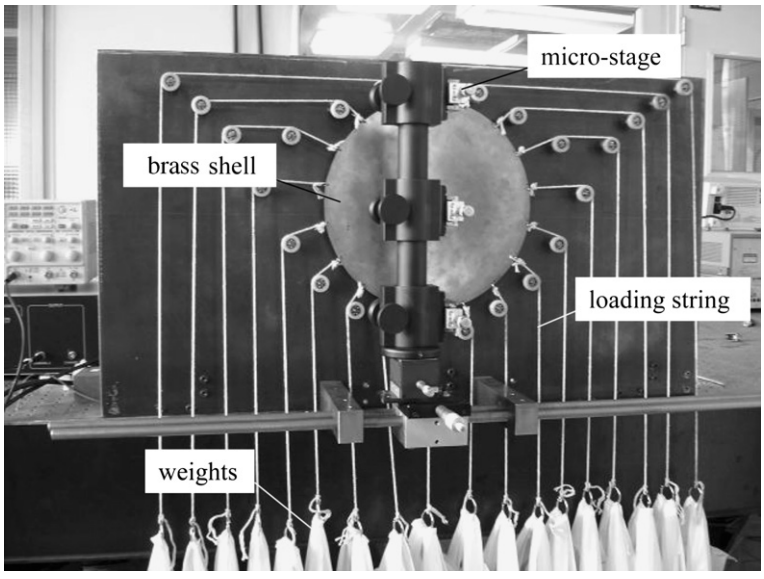

Fig. 8. Photograph of the experimental setup.

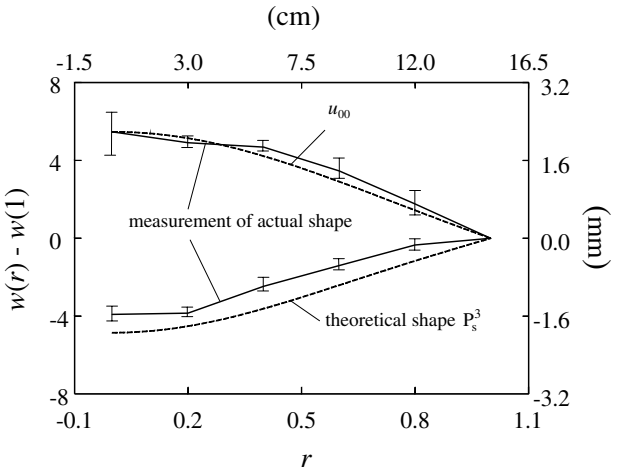

Fig. 9. Solid lines represent the measured radial shape in the initial position (upper branch) and strained position (lower branch) before edge tension is applied. Dashed lines represent the designed radial shape (u_{00}) and the theoretical radial shape of the strained position (P_s^3).

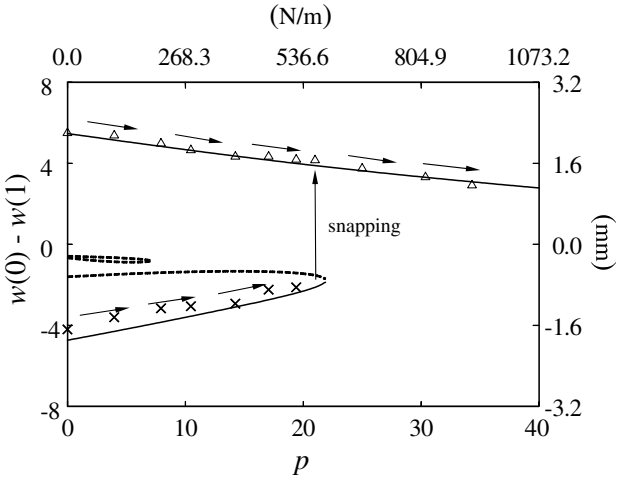

Fig. 10. Measured apex positions as functions of edge tension p.

9. Deformation measurement of a free shell under uniform tension

After measuring the initial shape of the shell, we start to put in equal weights (iron blocks) in the 18 plastic bags. The shell is first in the unstrained position. Ten different edge tensions are tested, they are $p = 3.97$, 7.94, 10.47, 14.25, 17.07, 19.41, 21.02, 25.00, 30.38, and 34.32. It is noted that these ten edge tensions are applied independently. For instance, after the application of the first loading $p = 3.97$, the shell was unloaded to reload the bags to the magnitude $p = 7.94$. We design a movable platform to support the bags of heavy weights at the bottom before tension is applied. After adjusting the weights the platform is then lowered gradually so that the tension can be applied to the outer rim of the shell almost at the same time. In this manner the tilting of the shell can be minimized. Under each loading condition, the deformation of the shell is measured in the same manner as described in the last section, except that only the relative heights at three diameters, instead of six, are measured. The mean values of the apex position are recorded with triangular symbols (△) in Fig. 10. After these measurements the shell is unloaded and bent gently by hand from the initial unstrained position to the strained position on the other side. The mean apex positions are then measured

in the same manner and the results are recorded in Fig. 10 as cross marks (×). At the seventh edge tension $p = 21.02$, the shell snaps back to the other side and the measurement stops at this point. The arrows in the figure indicate the deformation progression as the edge tension increases in both tests.

The solid (stable) and dashed (unstable) lines in Fig. 10 are the theoretical predictions of the axisymmetrical deformation as the edge tension is applied. Four modes are used in the calculation to ensure convergence. We found that the measured deflections agree with the theoretical predictions reasonably well in both the upper and lower branches. The actual reverse snapping speed is about 5% lower than the theoretical value.

Several comments can be added regarding this experiment. (1) The maximum stress resultants applied in the experiment is 34.32. This corresponds to the in-plane normal stress 2.3 MPa in the radial direction on the outer rim. This is well below the yield stress 70 MPa of brass. Therefore, the shell deformation in the experiment may be assumed to be elastic. (2) We have prepared more shells with slightly different initial heights. For these shells the theoretical prediction and experimental measurement all agree quite well. Therefore, the experimental result presented in Fig. 10 is typical and highly repeatable. (3) Generally speaking, if the initial height is less than 10 and circumferential deviation is smaller than 15% of the initial height, the discrepancy of the measured reverse snapping load is within 5% of the predicted value.

10. Conclusions

In this paper we study the deformation and stability of a shallow shell under uniform edge tension, both theoretically and experimentally. von Karman's plate model taking into account the membrane stretching due to bending deflection is adopted to formulate the equilibrium equations. Galerkin's method is used to discretize the differential equations of motion into a set of nonlinear algebraic equations. Although the initial shape of the shallow shell is assumed to be axisymmetrical, the possibility of unsymmetrical deformation is also examined. Both free and simply-supported boundary conditions are considered. Experiment on the free shell is conducted to verify the theoretical results. Several conclusions regarding the deformation of a shallow shell under uniform edge tension can be summarized in the following:

(1) In the case when the initial shape of the shallow shell is axisymmetrical, the equilibrium positions can be classified into axisymmetrical solutions and unsymmetrical solutions. For the unsymmetrical solutions both axisymmetrical and unsymmetrical assumed modes will be present. On the other hand, the axisymmetrical solutions contain no unsymmetrical assumed mode.
(2) All the unsymmetrical solutions are unstable. Therefore, they are not realizable in the laboratory. On the other hand, there may exist both stable and unstable axisymmetrical solutions.
(3) The addition of the unsymmetrical assumed modes in the solution does not affect the axisymmetrical solutions, neither the position nor the stability. Therefore, for quasi-static analysis, there is no need to include unsymmetrical assumed modes in the solution.
(4) If the shell is initially in the unstrained position, it will only be flattened smoothly when the edge tension is applied. No snap-through buckling is possible in this case. On the other hand, if the shell is initially in the strained position, it will be snapped back to the stable position on the other side of the base plane when the edge tension reaches a critical value.
(5) Experiment is conducted on brass shells to verify the theoretical predictions. Generally speaking, if the initial height is less than 10 and circumferential deviation is smaller than 15% of the initial height, the discrepancy of the measured reverse snapping load is within 5% of the predicted value.

References

Akkas, N., Odeh, F., 2001. A novel snap-through buckling behavior of axisymmetric shallow shells with possible application in transducer design. Computers and Structures 79, 2579–2585.

Ashby, M.F., Jones, D.R.H., 1980. Engineering Materials, An Introduction to Their Properties and Applications. Pergamon Press, Oxford.

Budiansky, B., Roth, R.S., 1962. Axisymmetric dynamic buckling of clamped shallow spherical caps. Collected Papers on Instability of Shells Structures. NASA TND-1510, pp. 597–606.

Chen, J.-S., Liao, C.-Y., 2005. Experiment and analysis on the free dynamics of a shallow arch after an impact load at the end. ASME Journal of Applied Mechanics 72, 54–61.

Chen, J.-S., Lin, C.-C., 2005. Axisymmetrical snapping of a spinning nonflat disk. ASME Journal of Applied Mechanics 72, 979–986.

Huang, N.C., 1964. Unsymmetrical buckling of shallow spherical shells. ASME Journal of Applied Mechanics 31, 447–457.

Huang, T.-M., 2006. Deformation and reverse snapping of a circular shallow shell under uniform edge tension. Master Thesis, Department of Mechanical Engineering, National Taiwan University, Taipei, Taiwan.

Simitses, G.J., 1990. Dynamic Stability of Suddenly Loaded Structures. Springer-Verlag, New York.

von Karman, T., Tsien, H.S., 1939. The buckling of spherical shells by external pressure. Journal of Aeronautical Science 7, 43–50.

Yamada, S., Uchiyama, K., Yamada, M., 1983. Experimental investigation of the buckling of shallow spherical shells. International Journal of Non-Linear Mechanics 18, 37–54.